Spatiotemporal toroidal waves from the transverse second-harmonic generation

Solomon M. Saltiel,[1,2] Dragomir N. Neshev,[1] Robert Fischer,[1] Wieslaw Krolikowski,[1,*] Ady Arie,[3] and Yuri S. Kivshar[1]

[1]*Nonlinear Physics Center and Laser Physics Center, Center for Ultra-high Bandwidth Devices for Optical Systems (CUDOS), Research School of Physical Sciences and Engineering, Australian National University, Canberra ACT 0200, Australia*

[2]*Department of Quantum Electronics, Faculty of Physics, Sofia University, Sofia BG-1164, Bulgaria*

[3]*School of Electrical Engineering, Faculty of Engineering, Tel-Aviv University, Tel-Aviv 69978, Israel*

**Corresponding author: wzk111@rsphysse.anu.edu.au*

Received October 17, 2007; revised January 17, 2008; accepted January 18, 2008; posted January 28, 2008 (Doc. ID 88721); published February 29, 2008

We study the second-harmonic generation via transversely matched interaction of two counterpropagating ultrashort pulses in $\chi^{(2)}$ photonic structures. We show that the emitted second-harmonic wave attains the form of spatially expanding toroid with the initial thickness given by the cross correlation of the pulses. We demonstrate the formation of such toroidal waves in crystals with random ferroelectric domains as well as in annularly poled nonlinear photonic structures. © 2008 Optical Society of America

OCIS codes: 190.0190, 190.4420, 260.5950.

Transverse second-harmonic generation (TSHG), i.e., emission of the second harmonic (SH) in the direction perpendicular to that of the fundamental wave, is a challenging nonlinear optical effect [1,2] that cannot be observed in bulk homogeneous nonlinear crystals since the phase matching condition cannot be satisfied. So far, the TSHG has been observed mostly in thin (1–2 μm thick) quantum-well waveguide structures [3–6]. Noncollinear SH generation has been recently observed in uniaxial strontium barium niobate (SBN) crystal with random distribution of ferroelectric domains. For the fundamental beam propagating along the z crystalline axis the SH was emitted in a form of a cone [7,8]. On the other hand, when the fundamental beam was propagating along the x or y crystallographic axis, the emission was taking place in all directions (including transverse) of a plane containing the fundamental wave [8–11]. However, if the single fundamental beam (pulse) propagates along the z axis, the TSHG phase-matching conditions cannot be fulfilled.

In this Letter, we report the observation of volume pure TSHG in a plane perpendicular to the z-directed fundamental beams. This is achieved by interaction of two counterpropagating femtosecond pulses along the optical axis of a quadratic nonlinear crystal. We observe the SH generated in the form of an expanding toroidal wave (T-wave) emitted from the overlap zone of the counterpropagating pulses.

Ferroelectric crystals with alternating sign of second-order nonlinearity provide effective means to quasi-phase-matched (QPM) nonlinear processes such as frequency doubling. While typically the light propagates in the crystallographic x–y plane, in our experiments we use fundamental beams directed along the optical z axis [Fig. 1(a)]. We use two different types of samples with $\chi^{(2)}$ spatial modulation: a 5 mm thick SBN crystal with naturally disordered domain structure [11] [Figs. 1(c) and 1(d)] and an annular periodically poled, z-cut, stoichiometric lithium tantalate (SLT) [12]. The SLT sample is 0.49 mm thick and the poling period is 7.5 μm [Fig. 1(f)].

In contrast to the fixed-period SLT structure, random distribution of antiparallel ferroelectric domains

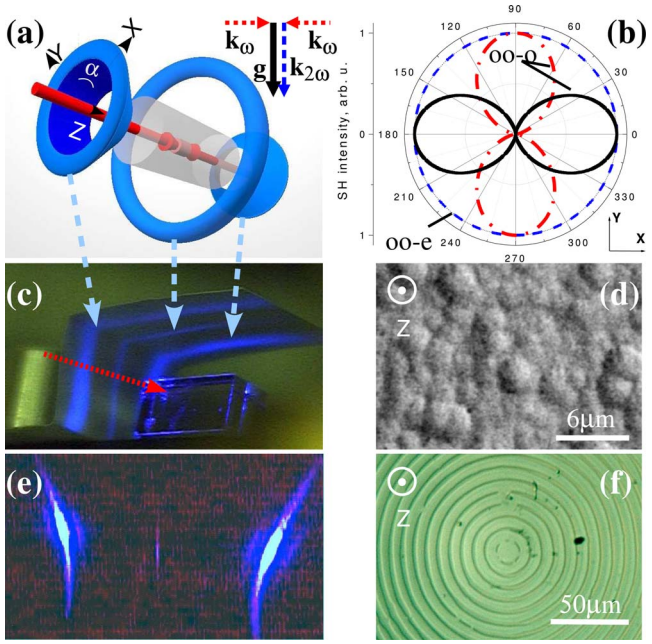

Fig. 1. (Color online) (a) Generation of SH T-waves with two counterpropagating beams. Inset, phase-matching diagram. (b) Theoretically determined emission diagram in polar coordinates (I_2, α) of a T-wave: dashed curve, phase-matched OO-E interactions (in SLT and SBN); dashed–dotted and solid curves, OO-O interaction (in SLT only) for both input polarizations either parallel along x or y (solid) or mutually perpendicular along x and y directions (dashed–dotted). (c) SH signal (emitted from SBN) as seen on the rectangular screen around the crystal. The two outer traces are the conical waves, and the weaker central line represents the T-wave. (d) Domain structure in as-grown SBN sample [11]. (e) Experimental image of a T-wave (central trace) and conical waves generated in the SLT sample. (f) Photo of the annular periodic domain pattern in SLT.

of an as-grown SBN leads to a natural disordered photonic structure [Fig. 1(d)]. This structural disorder provides almost a continuous set of grating vectors in the $x-y$ plane of the crystal allowing to phase match parametric processes over a broad range of frequencies [8,13].

As we already noted TSHG cannot take place for the fundamental beam propagating along the z axis. Instead, each pulse emits continuously a SH signal in the form of a cone [7,8], as shown schematically by the cones on both sides of the crystal in Fig. 1(a). These cones are clearly seen in the experiments with SBN as two strong outer lines shown in Fig. 1(c). Analogous conical emission takes place in the annular periodically poled sample of SLT [see two sidelines in Fig. 1(e)] [14]. The two cones are formed independently of the alignment of the two oppositely directed beams. Only when the two beams are exactly overlapped is a transverse second-harmonic wave radiated. In such case the momenta of the two counterpropagating photons cancel out, and the transverse phase matching can be achieved due to the reciprocal grating vector provided by the nonlinearity modulation. This can be seen clearly from the phase-matching diagram shown in the inset of Fig. 1(a). The solid arrow represents the effective reciprocal lattice vectors $\mathbf{g}$, while the dotted (red online) and the dashed (blue online) arrows denote the fundamental $\mathbf{k}_{\omega}$ and SH $\mathbf{k}_{2\omega}$ wave vectors, respectively. Due to these phase-matching restrictions the SH is emitted only from the region of pulse overlap and only for the duration of the pulse interaction. It is exactly this spatiotemporal overlap that allows for the emission of a spatiotemporal wave of a toroidal shape [illustrated by the central ring in Fig. 1(a)]. The width and intensity profile of this wave along the z direction is determined solely by the temporal correlation of the fundamental pulses, while the width and intensity profile in the transverse $(x-y)$ direction (propagation direction of the T-wave) depends on pulse length and the fundamental beams spatial profiles.

In our experiments we use pulses from a regenerative Ti:sapphire amplifier operating at a wavelength of 830 nm. The system delivers linearly polarized 165 fs long pulses of energy up to 3 μJ at a repetition rate of 250 kHz. The beam with a Gaussian spatial profile is split in a polarizing beam splitter and directed from both sides to a quadratic nonlinear medium such that the same pulses meet roughly in the center of the sample. A set of $\lambda/2$ plates allows the control of the relative powers of both beams and their polarizations. The average beam power before the beam splitter is $\sim$340 mW. The two beams are loosely focused in the sample to 160 μm waist. All facets of both samples are polished, and the emitted SH signal is recorded by a CCD camera.

The first-order TSHG phase matching requires very fine grating periods. For the SLT sample, the necessary period is 183 nm for a 830 nm fundamental wave. As the grating period of our SLT sample is 7.5 μm, the observed TSHG is thus due to a 41st-order phase matching, which, to the best of our knowledge, is the highest QPM order in crystals reported so far [1]. Naturally, such a high-order process results in a very low efficiency (well below 10^{-4}%).

The quadratic dependence of the SH signal on the power of the fundamental wave is verified by measuring the SH intensity in a particular single direction. To obtain angularly symmetric TSHG in the SLT sample, it is essential to focus both counterpropagating beams exactly at the center of the annular domain structure. In contrast, the TSHG in SBN does not depend critically on the position of the beams in the sample since the phase-matching conditions are the same everywhere in the crystal. Furthermore, since the average domain size is approximately 2.5 μm, the phase-matching order is 14, resulting in higher SH generation efficiency compared with that of SLT.

As different nonzero values of the $\chi^{(2)}$ tensor components are involved in TSHG in SBN and SLT, the emission diagrams for both structures are also different. The calculated emission diagrams in polar coordinates (I_2, α), where α is the emission (observation) angle for the ordinary and extraordinary polarized T-waves, are shown in Fig. 1(b). In the case of the OO-E interaction (ordinary polarized fundamental beams and extraordinary polarized SH), the relevant nonzero $\chi^{(2)}$ components in both crystals are d_{zxx} and $d_{zyy}=d_{zxx}$. The generated T-wave is polarized along the z axis of the crystal, and its intensity is constant for all emission directions in the $x-y$ plane. However, the SH intensity depends critically on the polarization of the fundamental waves $I_{2,ex} \propto [d_{zyy} I_1 \cos(\gamma_1 - \gamma_2)]^2$, where γ_1, γ_2 denote the angles of input polarizations for both the beams measured counterclockwise with respect to the x axis. In contrast to SBN where the OO-O (ordinary polarized fundamental beams and ordinary polarized SH) interaction is impossible, in SLT the relevant $\chi^{(2)}$ components d_{yyy} and $d_{yxx}=-d_{yyy}$ allow for the generation of an ordinary SH with its intensity varying with the emission angle α and input polarization directions as $I_{2,o} \propto [d_{yyy} I_1 \cos(\gamma_1+\gamma_2-\alpha)]^2$.

Experimental emission traces are shown in Fig. 1(c) for SBN $(0 \le \alpha \le \pi)$ and in Fig. 1(e) for SLT $(\alpha=\pi)$. However, since our samples are not cylindrical, it was not possible to measure accurately the angular variations of the intensity of SH. Instead, we measured the SH intensity and polarization properties of the emitted wave along the x and y axes of the crystal versus the polarization angles γ_1, γ_2. The experimental results for both SBN and SLT crystals are shown in Fig. 2 together with the curves representing theoretical fit. The graphs in Fig. 2(a) show the measured SH signal emitted in the SBN crystal (points) as a function of γ_1 for few values of γ_2. The agreement with the expression for $I_{2,e}$ (solid curves) of the OO-E interaction is excellent.

For the SLT crystal the polarization dependencies are more complicated due to the simultaneous contribution of both OO-O and OO-E interactions [see Figs. 2(b) and 2(c)]. Figure 2(b) shows the dependence of the total intensity of the SH signal on the polariza-

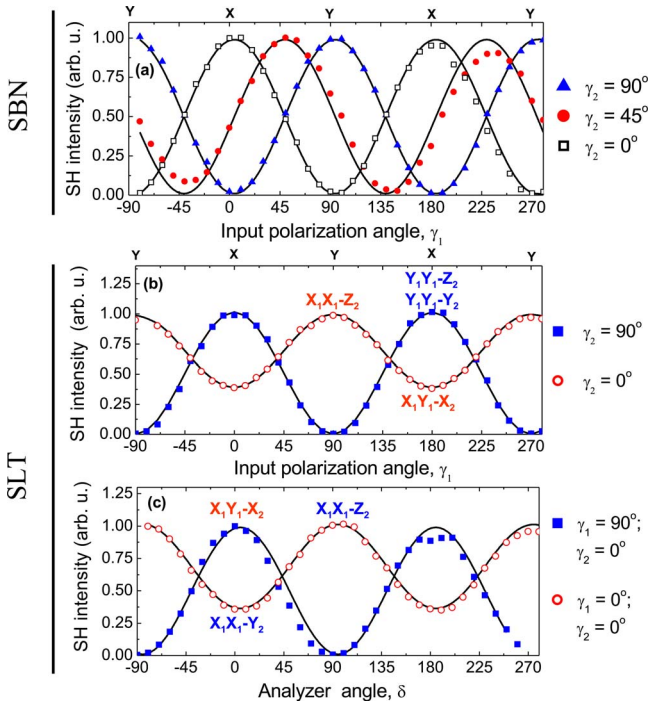

Fig. 2. (Color online) Polarization characteristics of SHG in (a) SBN and (b, c) SLT: (a) intensity of the SH signal as a function of the input polarization angle γ_1 for three values of γ_2, (b) total SH signal in the SLT sample as a function of the input polarization angle γ_1 for indicated values of γ_2, (c) intensity of the SH signal generated in the SLT sample as a function of the angle (δ) of an analyzer mounted in front of the CCD camera. In all plots solid curves represent the theoretical fits.

tion of the fundamental beams. On the other hand, in the case displayed in Fig. 2(c) both fundamental beams were either parallel (x direction, circles) or orthogonally (x and y directions, squares) polarized. The SH signal is then measured as a function of the angular position (δ) of the analyzer mounted in front of the CCD camera. For parallel polarized fundamental beams, both OO-E and OO-O processes contribute to the SH signal. Hence the recorded signal contains both ordinary and extraordinary components and never vanishes. For orthogonally polarized input beams, the SH wave is ordinary polarized (due to OE-O process), and the recorded SH signal vanishes at the angles $\delta=(-\pi/2,\pi/2,3\pi/2)$.

A quantitative analysis of the experimental data [Figs. 2(b) and 2(c)] indicates that the contribution of the OO-E process governed by the d_{zyy} component is stronger than that of the OO-O process governed by the d_{yyy} component. This does not agree with the value $d_{zyy}/d_{yyy}=0.59$ reported earlier [15]. This contradiction can be explained by the fact that the OO-E process is closer to the exact phase-matching condition than that of the OO-O process.

Due to the transverse geometry of the parametric interaction, the TSHG signal effectively translates the time coordinate into the space coordinate such that the width of the T-wave in the direction of the z axis is exactly the autocorrelation function of the interacting pulses [3,4,9]. From calibrated experimental photo similar to one in Fig. 1(e) we measured the thickness of the T-wave in SLT crystal to be 34 μm, which corresponds to 160 fs assuming secant hyperbolic temporal shape. Since the beam size is much bigger than the spatial extent of the pulse, the thickness of the T-waves in the propagation direction outside the sample is determined by the beam size and is about 250 μm.

In conclusion, we have generated toroidal second-harmonic waves via interaction of counterpropagating femtosecond pulses in annularly poled SLT structures and SBN crystals with disordered domains. As the thickness of the T-wave is determined by the correlation function of the fundamental pulses, this effect can be used as a background-free single short-pulse autocorrelator.

This work was supported by the Australian Research Council and the Israeli Science Foundation (grant 960/05). We thank D. Kasimov, A. Bruner, P. Shaier, and D. Eger for the SLT sample, and Jose Garcia Solé for a photo of the SBN domain structure.

References

1. X. Gu, R. Y. Korotkov, Y. J. Ding, J. U. Kang, and J. B. Khurgin, J. Opt. Soc. Am. B **15**, 1561 (1998).
2. G. D. Landry and T. A. Maldonado, J. Opt. Soc. Am. B **21**, 1509 (2004).
3. R. Normandin, R. L. Williams, and F. Chatenoud, Electron. Lett. **26**, 2088 (1990).
4. N. D. Whitbread, J. A. R. Williams, J. S. Roberts, I. Bennion, and P. N. Robson, Opt. Lett. **19**, 2089 (1994).
5. A. Fiore, Y. Beaulieu, S. Janz, J. P. McCaffrey, Z. R. Wasilewski, and D. X. Xu, Appl. Phys. Lett. **70**, 2655 (1997).
6. T. M. Crawford, C. T. Rogers, T. J. Silva, and Y. K. Kim, Appl. Phys. Lett. **68**, 1573 (1996).
7. A. R. Tunyagi, M. Ulex, and K. Betzler, Phys. Rev. Lett. **90**, 243901 (2003).
8. R. Fischer, S. M. Saltiel, D. N. Neshev, W. Krolikowski, and Yu. S. Kivshar, Appl. Phys. Lett. **89**, 191105 (2006).
9. R. Fischer, D. N. Neshev, S. M. Saltiel, A. A. Sukhorukov, W. Krolikowski, and Yu. S. Kivshar, Appl. Phys. Lett. **91**, 031104 (2007).
10. J. Trull, C. Cojocaru, R. Fischer, S. Saltiel, K. Staliunas, R. Herrero, R. Vilaseca, D. N. Neshev, W. Krolikowski, and Yu. Kivshar, Opt. Express **15**, 15868 (2007).
11. J. J. Romero, D. Jaque, J. Garca Solé, and A. A. Kaminskii, Appl. Phys. Lett. **78**, 1961 (2001).
12. D. Kasimov, A. Arie, E. Winebrand, G. Rosenman, A. Bruner, P. Shaier, and D. Eger, Opt. Express **14**, 9371 (2006).
13. J. J. Romero, C. Arago, J. A. Gonzalo, D. Jaque, and J. Garcia Solé, J. Appl. Phys. **93**, 3111 (2003).
14. S. M. Saltiel, D. N. Neshev, R. Fischer, W. Krolikowski, A. Arie, and Yu. S. Kivshar, arXiv.org e-print archive (August 25, 2007), http://arxiv.org/abs/0708.3417v1.
15. F. Charra and G. G. Gurzadyan, in *Nonlinear Dielectric Susceptibilities*, D. F. Nelson, ed. (Springer, 2000).